09

Characteristics of harmonics generated by oblique incidence of a relativistic laser beam on an inhomogeneous plasma

© A.A. Andreev[1,2], K.Yu. Platonov[3]

[1] St. Petersburg State University, St. Petersburg, Russia
[2] Ioffe Institute, St. Petersburg, Russia
[3] Peter the Great Saint-Petersburg Polytechnic University, St. Petersburg, Russia
e-mail: konstantin_platonov@yahoo.com

Received September 21, 2023
Revised December 31, 2023
Accepted April 12, 2024.

Self-consistent focusing of high harmonics of a relativistic intensity femtosecond laser pulse reflected from a plasma surface is considered. The studied harmonics are summed into a sequence of short intense pulses (attopulses). The plasma parameters (density, inhomogeneity scale) and the laser pulse (intensity, transverse profile) necessary to obtain a given focusing distance of attopulses are determined. The radius of the focusing spot and the intensity of attopulses at the focal point are determined.

Keywords: super strong laser fields, attopulses, self-focusing.

DOI: 10.61011/EOS.2024.09.60044.5428-24

Introduction

Reflection of a relativistic intense short laser pulse from a solid-state target results in generation of several ultrashort pulses of attosecond duration (atto-pulses), consisting mainly of higher order harmonics of laser frequency [1]. Such pulses are generated due to vibrations of the reflective electron layer in the target with a relativistic velocity [2]. Atto-pulses are promising for use in X-ray imaging of ultrafast processes, therefore, it is relevant to study the formation and propagation of such pulses from the laser target to the studied object without increasing the duration and decreasing the intensity. One of the ways to implement such capabilities is to focus the radiation reflected from the target at large (hundreds of micrometers) distances. It is known that a laser pulse of relativistic intensity leads to penetration through a plasma target and formation of a concave reflective surface [3]. With the appropriate selection of parameters, the focal distance of such a mirror can be large enough to allow localization (focus) atto-pulses in a small area of space at a great distance from the laser target [4]. In paper [4] normal incidence of a laser pulse with a plane phase front onto a target is discussed. The present study is aimed at determining the focusing conditions of the reflected pulse with an oblique incidence and displacement of the focus point of the incident laser beam relative to the target surface (curved phase front).

Spatial profile of the reflecting surface

High laser intensities are achieved by focusing the propagating laser beam in a vacuum chamber. Ideally, the target is positioned in the middle of the focal waist, thereby achieving maximum possible laser intensity on the target. In real conditions (as well as in order to change the intensity), the focus point can be located in front of or behind the target at a distance of units and tens of micrometers. In this case the pulse with a curvature similar to the phase front will be reflected from the target. By changing the distance from the focus point to the target, different values of the front curvature radius may be obtained, which, in combination with the target curvature radius, allows „adjusting“ the reflection process to different focusing distances. The shape of the target's reflecting surface is determined by the balance of forces of the ponderomotive pressure of laser pulse and ambipolar plasma field. The profile of the reflecting surface (critical density profile) is influenced by such laser parameters as intensity, transverse profile, phase front curvature and angle of incidence of the laser beam, as well as the density and scale of spatial heterogeneity of laser plasma. All these factors may be thoroughly considered in numerical PIC modeling of the density profile of a laser target.

An example of spatial distribution of electron density obtained through numeric 2D PIC-modelling with the use of PSC code [5], is shown in Fig. 1, *a*. The following modelling parameters were used: laser intensity $6.7 \cdot 10^{19}$ W/cm^2, duration $\tau_L = 33$ fs, target SiO_2, target density $n_{i0} = 2 \cdot 10^{22}$ cm^{-3}, levels of ionization Si^{+12}, O^{+8}, scale of plasma heterogeneity $L = 0.25\,\mu$m, laser beam radius $w_L = 1.5\,\mu$m. Incident angle 45°, *P*-polarization. The axis of laser beam corresponded to $y_0 = 20\,\mu$m in Fig. 1, *a*. The initial front of the laser pulse was planar ($z = \text{const}$). The moment of time in Fig. 1, *a* corresponded to reflection 8 and 13 of laser pulse periods. Fig. 1, *a* shows that electron density is penetrated in the direction of the ponderomotive pressure force of a laser pulse, where the asymmetry of the reflecting surface is observed, which

increases with the growth of intensity, and Fig. 1, *b* shows an option of the model approximation of the numerically computed blue curve in Fig. 1, *a*.

Taylor expansion of the density profile Fig. 1, *a* represents a parabola:

$$z(y) = -z_e\left(1 - \frac{(y - y_0 - y_e)^2}{(w_L/\cos\theta - y_e \mathrm{sign}(y - y_0 - y_e))^2}\right). \quad (1)$$

We assume that: $kz_e \ll 1$, $kL \ll 1$, where $k = \omega_L/c = 2\pi/\lambda_L$ — wave vector of laser pulse with a frequency of ω_L. The shifts z_e, y_e of electron density profile can be found from the equations of force balance and momentum flow. The ponderomotive pressure force of laser pulse on the electron density of the target has a non-zero time average component: $\mathbf{F} = (e[\mathbf{v_e} \times \mathbf{B}]/c$ (on the target surface $B = (a_0(1 + R)m_e\omega c/e$, where R — amplitude reflectance factor). The components of this force are balanced by the ambipolar forces that arise due to the shift in electron density. Dimensionless z-component of ambipolar field

$$E_z = Zk\int_{-\infty}^{z_e}(n_i(z)/n_{\mathrm{cr}})dz$$

is balanced by z-component of the light pressure force:

$$(R + 1)a_0\cos\theta = k\int_0^{z_e}(n_i(z)/n_{\mathrm{cr}})dz.$$

Where at $n_i(z) = n_{\mathrm{cr}}\exp(z/L)$, $z \in [0; L\ln(Zn_{i0}/n_{\mathrm{cr}})]$; $n_i(z) = Zn_{i0}$, $z \in [L\ln(Zn_{i0}/n_{\mathrm{cr}}); +\infty)$ we obtain the estimate of the target surface penetration depth:

$$kz_e = kL\ln\left(1 + \frac{(R + 1)a_0\cos\theta}{kL}\frac{n_c}{Zn_{i0}}\right)$$

$$\text{at } kL \geq \left(\frac{n_c}{Zn_{i0}}\right)^2(R + 1)a_0\cos\theta, \quad (2)$$

$$kz_e = \left(\frac{n_c}{Zn_{i0}}\right)\left((R + 1)a_0\cos\theta - kL\frac{Zn_{i0}}{n_c}\right)$$

$$\text{at } kL \leq \left(\frac{n_c}{Zn_{i0}}\right)^2(R + 1)a_0\cos\theta.$$

Since usually $Zn_{i0}/n_c > 10^2$, $a_0 < 10^2$, top line (2) corresponds to the range of heterogeneity scale L from tens of nanometers and above, and only for $L \sim$ a few nanometers, the bottom line is valid (2). Further, we'll assume the upper inequality fulfilled. The dimensionless y component of the light pressure force is balanced by y component of the ambipolar electric field:

$$(R + 1)a_0\sin\theta = ky_eZn_i(z_e)/n_{\mathrm{cr}},$$

from where

$$ky_e = \frac{(R + 1)a_0\sin\theta n_{\mathrm{cr}}}{Zn_i(z_e)}. \quad (3)$$

Formulae (1)–(3) define the modelled profile of the reflection surface in the form of an asymmetric parabola. The top line of the formula (2) up to replacement $(R + 1)\cos\theta \leftrightarrow 2(1 + \sin\theta)$ coincides with the evaluation of [4], which considered the symmetrical shape of the reflection surface ($y_e = 0$). For sufficiently long pulses (≥ 100 fs), there will be a significant shift in the ion density along with the electron density. To estimate the shift of the ion density profile, consider the momentum flow balance equation for the pulse incident on a laser radiation target with a time-average intensity of I_L:

$$2n_im_iv_i^2 = (1 + R)I_L\cos\theta/c.$$

From the balance equation, a differential equation is obtained that determines the position of the boundary of moving ions:

$$\frac{v_i(t)}{c} = \frac{\partial z_i(y, t)}{\partial t} = \sqrt{(a^2(0, y, t))_{T_L}}\sqrt{\frac{(1 + R)m_en_{\mathrm{cr}}\cos\theta}{2Am_in_i(z_i(y, t))}},$$

where the brackets $\langle\ \rangle_{T_L}$ denote an averaging of the squared field over the laser period T_L. For the exponential density profile in the vicinity of the critical concentration (radiation reflection point) $n_i(z) = (n_{\mathrm{cr}}/Z)\exp(z/L)$, the differential equation is written as follows

$$z_i = 2L\ln\left(1 + a_0\tau_L\sqrt{\frac{Zm_ec^2(R + 1)}{16Am_pL^2\cos\theta}}\right). \quad (4)$$

Total penetration depth of the target is composed by summing up the formulae (2) and (4): $z_T = z_e + z_i$, while the formula of the reflecting surface is defined by the ratio (1) with replacement of $z_e \to z_T$.

Reflection of a laser pulse with a curved phase front from a concave target

It is convenient to describe an obliquely incident laser pulse in an inclined coordinate system: $\tilde{z} = -z\cos\theta + y\sin\theta$, $\tilde{y} = y\cos\theta + z\sin\theta$, the axes of which are shown in Fig. 1, *b*. The dimensionless vector potential of the laser field propagating along the axis $\tilde{z}$ in Fig. 1, *b*, in the paraxial approximation near the focus point $\tilde{z} = \tilde{z}^*$ is expressed as

$$a(\tilde{z}, \tilde{y}, t) = a_0\exp\left(-\frac{(\tilde{z} - ct)^2}{c^2\tau_L^2}\right)\sqrt{\frac{w_L}{w(\tilde{z} - \tilde{z}^*)}}$$

$$\times\exp\left(-\frac{\tilde{y}^2}{w(\tilde{z} - \tilde{z}^*)^2}\right)\cos\left(k(\tilde{z} - \tilde{z}^*) - \omega t\right.$$

$$\left. - \frac{k\tilde{y}^2}{2\sigma(\tilde{z} - \tilde{z}^*)} + \eta(\tilde{z} - \tilde{z}^*)\right), \quad (5)$$

$$w(\tilde{z}) = w_L\sqrt{1 + \frac{\tilde{z}^2}{z_R^2}},\quad \sigma(\tilde{z}) = \tilde{z} + \frac{z_R^2}{\tilde{z}},$$

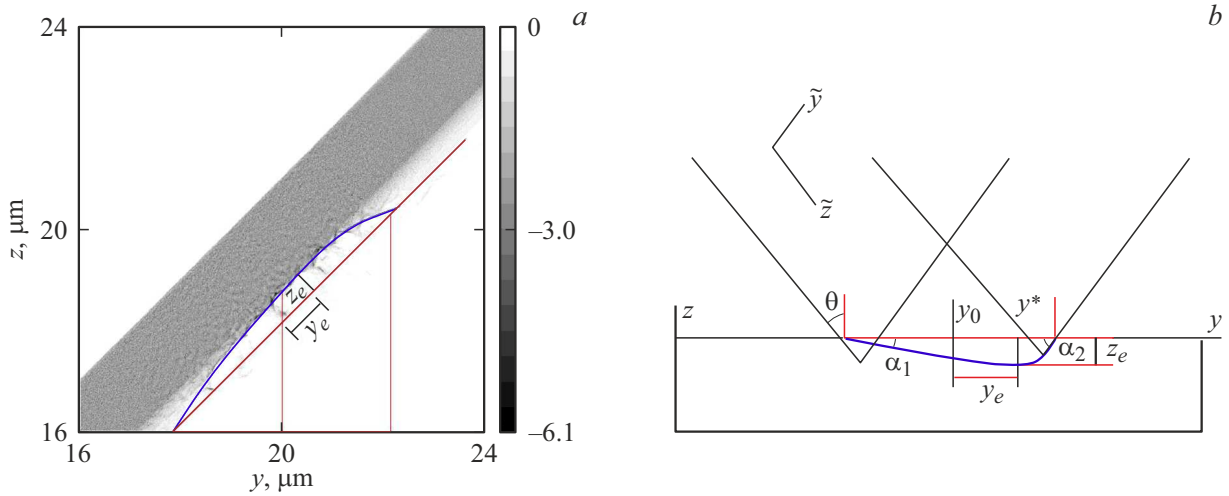

Figure 1. *a* — numerical modelling of the electron density profile when the laser pulse is reflected from a plane target; *b* — model profile of the reflection surface.

$$\eta(\tilde{z}) = 0.5\,\mathrm{atan}\left(\frac{\tilde{z}}{z_R}\right).$$

Here $w_L = w(\tilde{z} = \tilde{z}^*)$ — minimal half-width of the laser beam, $z_R = (kw_L^2)/2$ — Rayleigh length, $a_0 = eE_L/m\omega c$, τ_L — , respectively, the dimensionless amplitude and time duration of the laser pulse. Function $w(\tilde{z})$ describes the local (in point $\tilde{z}$) half-width of the laser beam, function $\sigma(\tilde{z})$ — local radius of the phase front curvature. When a laser pulse (5) impacts the opaque quasi-neutral plasma with an initial particle density profile $n_e(z) = Zn_i(z) = Zn_{i0}\exp(-z/L)$, the electron and ion densities become penetrated, as a result of which electrons are displaced by distances z_e, y_e along the axes (z, y), and reflection occurs from the density profile (1). When a *P*-polarized laser pulse obliquely falls on a target, a periodic structure of sections appears on its surface where the normal component of the electric field extracts electrons from the surface into vacuum [6]. As a result, electron jets appear, observed, for example, in Fig. 1, *b*, and the reflection surface itself becomes wavy. The density profile consisting of the two branches of parabola (1) has two focusing distances $f_{p1,2}$, specific average focusing distance f_{pt} and inter-focus distance δf_p:

$$f_{p1,2} = \frac{(w_L/\cos\theta \pm y_e)^2}{4z_T},\quad f_{pt} = \frac{f_{p1} + f_{p2}}{2},$$

$$\delta f_p = f_{p1} - f_{p2} \approx \frac{y_e w_L}{z_T \cos\theta}. \qquad (6)$$

Formulae (6) for estimating the focusing parameters of a curved surface will be valid up to a numerical multiplier for a reflecting surface of arbitrary shape, since the angles $\alpha_{1,2}$ in Fig. 1, *b* are estimated as $\alpha_{1,2} \approx z_T/(w_L/\cos\theta \pm y_e)$, and $f_{p1,2}$ — respectively as $(w_L/\cos\theta \pm y_e)\alpha_{1,2} = (w_L/\cos\theta \pm y_e)^2/z_T$, and only numerical factor in this estimate depends on the surface shape. In Appendix 1, the case of a triangular plasma recess is considered more carefully and the focusing distance for such a profile is calculated.

In Fig. 2, *a* the curve (6) is shown in orange color for $a_0 = 2.2$, blue color — curve for $a_0 = 0.7$. The circles and squares of the corresponding color stand for the computation data [7], when $z_T \approx z_e$, $\theta = 0$ and $z^* = 0$. It can be seen that for $a_0 > 1$, the estimate (6) of the focusing distance adequately describes the numerical modelling data, and the focusing distance for small deflection angles $\alpha_{1,2}$, with an accuracy of a unit multiplier, does not depend on the choice of the functional type of the plasma density profile. In Appendix 1, the triangular profile of the reflection surface is considered and it is shown that formula(6) for the focusing distance is also valid for such a profile. In Fig. 2, *b* it is also shown that the focusing distance f_{pt} versus incident angle θ in formula (6) also corresponds to the numerical modelling data.

Focusing of the generated harmonics

The reflected pulse, unlike the incident pulse, contains a set of high-frequency harmonics with wavelengths $\lambda_n = \lambda_L/n$. Harmonics arise due to the relativistic motion of the reflecting electronic surface. The harmonics are summed up in a sequence of short intense pulses (atto-pulses) shown below. The numbers of harmonics lie within the interval $n \in [1; n_{\max}]$. Number $n_{\max}$ of the maximal reflected harmonic may be obtained from [8], where the duration τ_{atto} of the atto-pulse reflected from a sharply bounded bulk target is estimated. Obviously, $n_{\max} \approx T_L/2\tau_{\mathrm{atto}}$; having taken from [8] the formula for τ_{atto}, we'll get the following

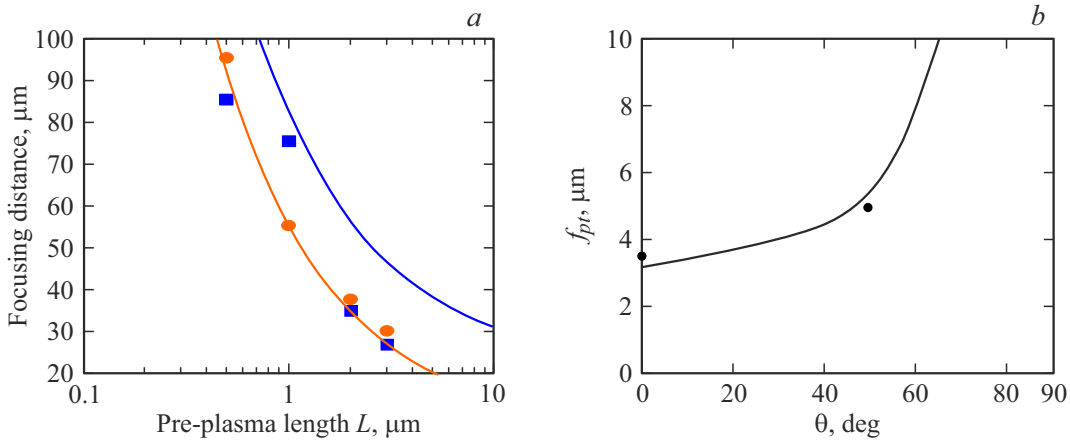

Figure 2. (*a*) Focusing distance f_{pt} versus the heterogeneity scale of the laser target plasma $Si^{+12}O^{+6}$ with a density of $Zn_{i0} = 50n_c$ for the laser pulse intensities 10^{18} W/cm^2 ($a_0 = 0.7$) — blue curve and 10^{19} W/cm^2 ($a_0 = 2.2$) — orange curve, circles and squares — data of PIC-computation [7]. (*b*) Focusing distance f_{pt} versus incident angle θ: solid line — formula (6) for f_{p1}, dots — computation results for the laser intensity 10^{22} W/cm^2, target Au^{+50}, $n_{i0} = 6 \cdot 10^{22}$ cm^{-3}, $L = 0.25\,\mu$m, $w_L = 2.5\,\mu$m.

estimate:

$$n_{\max} \approx \frac{a_0^2 N(1-\sin\theta)}{2C\cos^2\theta}\left(\sin\theta + 4\cos^3\theta\sqrt{\frac{N^2}{a_0^2} - \frac{a_0^2\sin^2\theta}{N^2(1-\sin\theta)^2}}\right), \quad (7)$$

$$N = \frac{n_e}{n_{\rm cr}}, \quad a_0 > 1, \quad \frac{a_0}{N} < 1,$$

where $C \sim 1$ — numerical constant. The applicability of the sharp boundary condition limits the scale of plasma heterogeneity: $kL \le (\frac{n_c}{Zn_{i0}})^2(R+1)a_0\cos\theta$ (bottom line (2)). If the sharp boundary condition is not fulfilled (our case), the dimensionless concentration of N in formula (7) is taken on the reflection surface:

$$N = \frac{n_e(z_e)}{n_{\rm cr}} = \begin{cases} \exp(z_e/L, & z_e \le L\ln(Zn_{i0}/n_{\rm cr}), \\ Zn_{i0}/n_{\rm cr}, & z_e L\ln(Zn_{i0}/n_{\rm cr}), \end{cases}$$

as a result of which the dependence of $n_{\max}$ on the heterogeneity scale $n_{\max}(L)$ appears. Formula (7) is valid for a plane surface, curvature makes a small contribution and can be taken into account by introducing a local angle of incidence $\tilde\theta(y) = \theta + \mathrm{atan}(dz(y)/dy)$ and subsequent averaging along the coordinate y within the laser spot on the plasma surface:

$$(2w_L/\cos\theta)^{-1}\int\limits_{-w_L/\cos\theta}^{w_L/\cos\theta} n_{\max}(\tilde\theta(y))dy.$$

Since the incident angle is small $dz(y)/dy < 1 \forall y$, the procedure of averaging at $\theta \sim 1$ practically will not change the value (7). At $\theta \ll 1$ Taylor's series (7) expansion is written as

$$n_{\max} \approx \frac{2a_0N^2}{C}\left(1 + \theta\left(\frac{a_0}{4N} - 1\right) + \ldots\right),$$

and the angle averaging procedure will include only change of the coefficient of θ linear summand, i.e. will not change the value (7) either. It should be noted that there's an optimal ratio a_0/N, at which the harmonics amplitudes$cn \sim n_{\max}$ are maximal. In paper [8] it was demonstrated that the interval $1/4 < a_0/N < 1$ and incident angles $45^\circ \le \theta \le 70^\circ$ are optimal from the standpoint of amplitude and duration of the atto-pulse formed by the high-frequency harmonics.

Size $2w_{rn}$ of the focal waist of n-th atto-pulse harmonic differs from the size $2w_L$ of the incident pulse waist and is sensitive to the functional profile $z(y)$ of the reflecting surface. For the parabola profile the focusing diffraction limit w_{rn} may be attained: $f_{pt}\lambda_n/w_L$. With a profile shape other than parabolic, the size of the focal waist will exceed the diffraction limit, for example, for a triangular density profile, the size of the focal waist is $2w_{rn}$: $w_L + y_e$ (Appendix 1 (p9)).

The amplitude of the n-th harmonic of the atto pulses at the focus point of the reflected laser pulse can be estimated as follows. From (5) it follows that the amplitude of the incident pulse on the target surface is $a_0(1 + 4k^2z^{*2}/k^4w_L^4\cos^2\theta)^{-1/4}$. Distribution by number n of amplitudes a_{rn} of the atto pulse on the target surface is expressed exponentially [8]:

$$a_{rn}|_{z\approx 0} \approx Ra_0\frac{n^{-p/4+1}(1 + 4k^2z^{*2}/k^4w_L^4\cos^2\theta)^{-1/4}}{\sqrt{\sum\limits_{n=1}^{n_{\max}} n^{-p/2+1}}}, \quad (8)$$

where the exponent p of the spectrum depends on the target parameters, including the heterogeneity scale. The denominator in (8) ensures the correct normalization of harmonic amplitudes so that

$$R_2 = \sum_{n=1}^{n_{\max}} a_{rn}^2(1 + (4k^2z^{*2}/k^4w_L^4\cos^2\theta)^{1/2}/a_0^2$$

was the reflectance from the target in terms of power. For the sharply-bounded bulk targets similar estimates have been given in various papers $p \in [2.5; 3]$ [9,10]. Further, we'll use $p \approx 2.5$. In paper [4] it was demonstrated that the characteristic radius of the spot generating the atto pulse harmonics for n ($n_{\max} \gg 1$) is $w_{\text{ef}} \approx 0.7w(z^*) = 0.7w_L\sqrt{1 + z^{*2}/z_R^2}$. At a distance of f_{pt} the spot area of n-th harmonic will make $S_{rn} = \pi w_{rn}^2$ (w_{rn} — spot radius of n-th harmonic in the point of focus). Accordingly, the amplitude a_{rn} of the harmonic of the reflected pulse at the focus point will be determined by the areas ratio and will be

$$\frac{a_{rn}}{a_0} = \frac{Rw_{\text{ef}}}{w_{rn}} \frac{n^{-p/4+1}(1 + 4k^2z^{*2}/k^4w_L^4\cos^2\theta)^{-1/4}}{\sqrt{\sum_{n=1}^{n_{\max}} n^{-p/2+1}}}$$

$$\approx \frac{0.7Rw_L\sqrt{1 + z^{*2}/z_R^2}n^{-p/4+1}}{(1 + 4k^2z^{*2}/k^4w_L^4\cos^2\theta)^{-1/4}w_{rn}\sqrt{\sum_{n=1}^{n_{\max}} n^{-p/2+1}}}. \quad (9)$$

The formula (9) allows estimating the amplitude of n-th harmonic of the atto pulse at the focus point at a given position of the laser beam focusing point z^* in front of the target and the heterogeneity scale L of laser plasma (taking into account $n_{\max}(L)$). The intensity of reflected harmonic radiation ($n > n^*$) in the point of focus $I_{\text{focus}}(n^*)$ is defined by the formula:

$$\frac{I_{\text{focus}}(n^*)}{I_0} = \frac{\sum_{n^*}^{n_{\max}}(a_{rn})^2}{a_0^2}, \quad (10)$$

where $I_0 = m_e^2c^3\omega_L^2a_0^2/4\pi e^2$ — intensity of the incident pulse.

To clarify w_{rn}, it shall be emphasized that the profile of the reflecting surface corresponds to a local equality at the points of hot electrons pressure surface $n_e(y, z)T_e$ and the ponderomotive pressure surface of laser field. When estimating the temperature of hot electrons $T_e \approx mc^2\left(\sqrt{1 + \langle a^2(y, z, t)\rangle_{T_L}} - 1\right)$, it turns out that the electron density profile repeats the profile of the laser field distribution on the plasma surface:

$$\frac{n_e(y, z)}{n_{\text{cr}}} \approx \frac{\langle a^2(y, z, t)\rangle_{T_L}}{4\pi\left(\sqrt{1 + \langle a^2(y, z, t)\rangle_{T_L}} - 1\right)}$$

$$\to \frac{\sqrt{\langle a^2(y, z, t)\rangle_{T_L}}}{4\pi} \text{ at } a^2 \gg 1. \quad (11)$$

It should be noted that the field and electron density are self-matched and $\langle a^2(y, z, t)\rangle_{T_L}$ in (11) depends on the density distribution n_e. For the estimates we may take $\langle a^2(y, z, t)\rangle_{T_L}$ of the incident pulse (5) (Gaussian profile in the system y', z'), and then the estimate of profile $n_e(y, z)$ will also be of Gaussian type. Near the maximum, the Gaussian distribution is approximated by a parabola, when focusing, the diffraction limit of focusing is reached w_{rn}: $2\pi f_{pt}/nkw_{\text{ef}}$. The possibility of focusing into a small region $w_{rn_{\max}} \sim \lambda_L/n_{\max}$ (at $f_{pt} \sim w_{\text{ef}}$) on an artificially prepared parabolic reflecting surface and obtaining at $n_{\max} \gg 1$ the intensities I_{focus} reaching Schwinger limit (vacuum breakdown) is outlined in [4.10]. The oblique incidence during self-focusing leads to an asymmetry of the parabola branches (a shift by y_e (3) of the parabola bottom point relative to the axis of the incident beam), which leads to a blurring of the focusing distance by δf_p. If the value δf_p is less than Rayleigh distance of n-th harmonic, $\delta f_p < \pi f_{pt}^2\lambda_n/w_{\text{ef}}^2$, then, the diffraction limit of the focusing spot radius estimate is preserved. Otherwise, $\delta f_p > \pi f_{pt}^2\lambda_n/w_{\text{ef}}^2$ minimal radius of the focusing spot of n-th harmonic is $w_{rn} \approx \sqrt{\delta f_p\lambda_n}$.

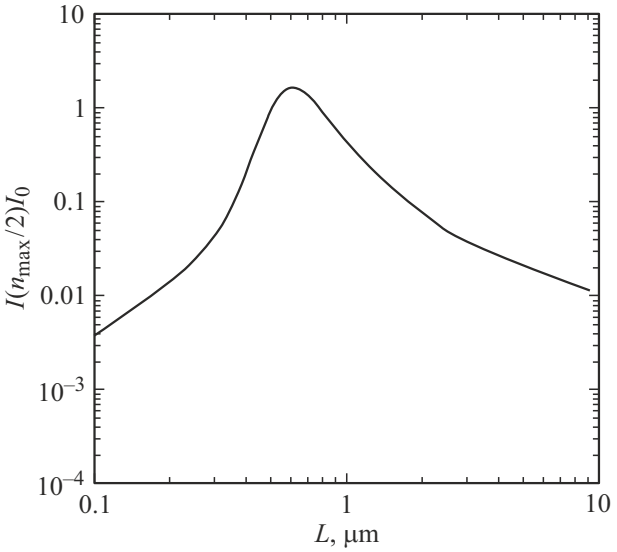

Figure 3. Dimensionless intensity of the high-frequency harmonics in focus $I_{\text{focus}}(n^* = n_{\max}/2)/I_0$ versus heterogeneity scale L at laser intensity $I_0 = 10^{22}\,\text{W/cm}^2$, $w_L = 2.5\,\mu\text{m}$, target Au^{+50}, $n_{i0} = 6 \cdot 10^{22}\,\text{cm}^{-3}$, $w_{rn} \approx \sqrt{\delta f_p\lambda_n}$. Other parameters of the target and laser pulse are shown in Fig. 2.

Fig. 3 illustrates the dimensionless intensity of the high-frequency harmonics in focus $I_{\text{focus}}(n^* = n_{\max}/2)/I_0$ as a function of the heterogeneity scale L for the laser intensity $I_0 = 10^{22}\,\text{W/cm}^2$, $w_L = 2.5\,\mu\text{m}$, target Au^{+50}, $n_{i0} = 6 \cdot 10^{22}\,\text{cm}^{-3}$ in case when $w_{rn} \approx \sqrt{\delta f_p\lambda_n}$. It can be seen that focusing with an asymmetric parabola makes it possible to increase the intensity of the „tail" of the reflected pulse spectrum ($n > n_{\max}/2$) up to the intensity of the incident pulse I_0. It should be noted that when focusing with a symmetric parabola (w_{rn}: $2\pi f_{pt}/nkw_{\text{eff}}$) maximal value $I_{\text{focus}}(n^* = n_{\max}/2)/I_0$ in Fig. 3 would be increased up to ≈ 40.

Away from the maximum of the incident Gaussian pulse (5), the approximation of Gaussian distribution is close to linear. Thus, the intensity distribution in the focal waist of the reflected pulse should contain a bright spot in the center and a periphery where the intensity is several

times higher than the intensity of the incident laser pulse. It should also be stressed that the angular divergence of individual harmonic$\theta_n \sim w_{rn}/f_{pt} \sim \lambda_L/nw_L$, similar to the half-width w_{rn}, coincide with the growth of n. Accordingly, the highest frequency harmonics composing the atto pulses propagate closer to the axis of the reflected beam. If there is a selection based on the angle of the reflected pulse, it is possible to separate the high-frequency part of the spectrum. A similar selection was carried out in the study [11], where the suppression of low-frequency harmonics due to angular selection led to a planer spectrum for the part of the reflected pulse propagating directly along the reflected beam axis as shown in Fig. p1.

To check and calibrate formulae (9), (10) the Appendix 2 provides the numerical modelling data [6]$I_{\text{focus}}(n^* = 1)/I_0$ of the dimensionless laser intensity at the focus point of all harmonics of the reflected laser pulse as a function of plasma heterogeneity scale L for the parameters of the laser pulse and target shown in Fig. 2. These data were compared with the model formulae (9), (10), triangular and trapezoidal (with equal link lengths) profiles of the target surface were used. The dependence of the reflected radiation intensity on the heterogeneity scale L, as in Fig. 3, has a local maximum, which is explained as follows. At $L = 0$ the reflection surface is plane and no focusing occurs, $w_{rn} \approx w_L$ (at that $I_{\text{focus}}(n^* = 1)/I_0 = R^2$). As L grows, the focusing occurs and$w_{rn} \ll w_L$. At higher L the value N drops in (7), which leads to decrease of $n_{\max}$ (number of summands in the sum (10)) and lower intensity in the point of focus. As a result in Fig. 3 and Fig. p3 the dependence is formed with a maximum.

Numerical modelling of laser beam focusing with a curved phase front

2D PIC computations were performed to verify the above estimates of the focusing distance and focusing parameters of the reflected pulse. Note that 2D computation includes only a narrow range of values of the unused third coordinate, according to which in a real situation (3D-computation) focusing also takes place. Accordingly, the focusing degree in 2D-computation will be a priori reduced compared to the 3D-computation. It is possible to estimate the degree of focusing in 3D-computation (which is unavailable due to limited computational capabilities) as a squared degree of focusing in 2D computations. In 2D-computation the laser intensity was 10^{22} W/cm^2, wavelength 800 nm, target Au^{+50}, with a density of $6 \cdot 10^{22}$ cm^{-3}. The scale of the exponential density heterogeneity on the front side was selected $0.25\,\mu$m, and the target thickness $3.5\,\mu$m. Radius (half-width) of laser beam $w_L = 2.5\,\mu$m. The computation step was 4 nm in spatial coordinates and 1.3 as in time, number of particles was 30 in the cell for ions and 90 for electrons. Pulse duration was $\sim \exp(-(z-ct)^2/z_L^2)$ with $z_L = 5.25\,\mu$m. In total the pulse contained $2 \times 5.25/0.8 = 13$ periods. Rayleigh distance in formula (5) used to set the pulse value was $z_R = \pi w_L^2/\lambda_L \approx 9\,\mu$m. Incident angle on the target was $\theta = 45^\circ$, p-polarization. At the initial moment of modelling, the center of the pulse was located at a distance of $|z^*| = 9\,\mu$m in front of the target. Thus, the parameter was $z^*/z_R \approx -1$ in Fig. 1. If the pulse was propagating freely (ideally reflected), its half-width at the running distance l would be $w(l) = 1.5\sqrt{1 + l^2/9^2}\,\mu$m. If the pulse has run $9\,\mu$m to the target and $9\,\mu$m after, then its half-width would rise more than twice as much. In real reflection, due to penetration through electron density, a focusing „mirror" is formed, capable of reducing the width of the pulse and even focusing it. According to formulae (6) of the model, the focusing distance of such mirror is $f_{pt} \approx 5\,\mu$m for the heterogeneity scale $L = 250$ nm in formulae (2), (4). The target's density profile at the moment of reflection of intensity maximum of the incident pulse ($t = 32$ fs) is shown in Fig. 4, *a*. Fig. 4, *b* illustrates laser pulses — incident at $t = 0$ (bottom insert) and reflected at $t = 42$ fs (moment when the pulse center is reflected). Efficient focusing distance in Fig. 4, *b* is $\approx 4\,\mu$m which is consistent with the above-mentioned estimate $f_{pt} \approx 5\,\mu$m. Also, in Fig. 4, *b* the lateral size of the focusing region is $2\,\mu$m at initial lateral size of the beam $2w_L = 5\,\mu$m. Figure 4, *b* shows that the reflecting surface is displaced during reflection: the „head" and „tail" of the reflected focused pulse in Figure 4, *b* are shifted along the axis z relative to each other. The dynamics of the reflecting surface generates intersecting fronts from different areas of the reflection surface, as seen in Fig. 4, *b*. Because of this, the half-width of the focusing region exceeds the diffraction limit (reflection by an ideal parabola) and is most adequately estimated by the triangular density profile model — formula (p9) of Appendix 1. This formula gives $|\text{CD}| \approx 2.8\,\mu$m, which is close to $2\,\mu$m Fig. 4, *b*. The intensity of the reflected radiation in the focusing region in Fig. 4, *b* makes ~ 3 of the incident radiation intensity. In the 3D-computation, the degree of focusing would increase to ~ 10, which is comparable to the 3D modeling data in paper [12] obtained with comparable laser pulse and target parameters. It should be noted that estimation by methods of geometric optics assumes the ideal quality of the reflecting surface and does not take into account the reflection other than specular and present in our case. In Fig. 4 formula (10) gives for parameters $n_{\max} \approx 350$ and the pulse duration of several attoseconds.

Two-pulse reflection scheme

Computations show that formation of a concave „mirror" continues at long distances after reflection of the first pulse because the density wave is moving inside the target. Figure 5 shows the electron density profile at a time of 90 fs for computation of Figure 1, *a*, when the reflected pulse left the modelling box. Fig. 5, *b* shows that at $y = 30\,\mu$m the second pulse has run $57\,\mu$m from the start point, and its diffraction divergence corresponds to the blue

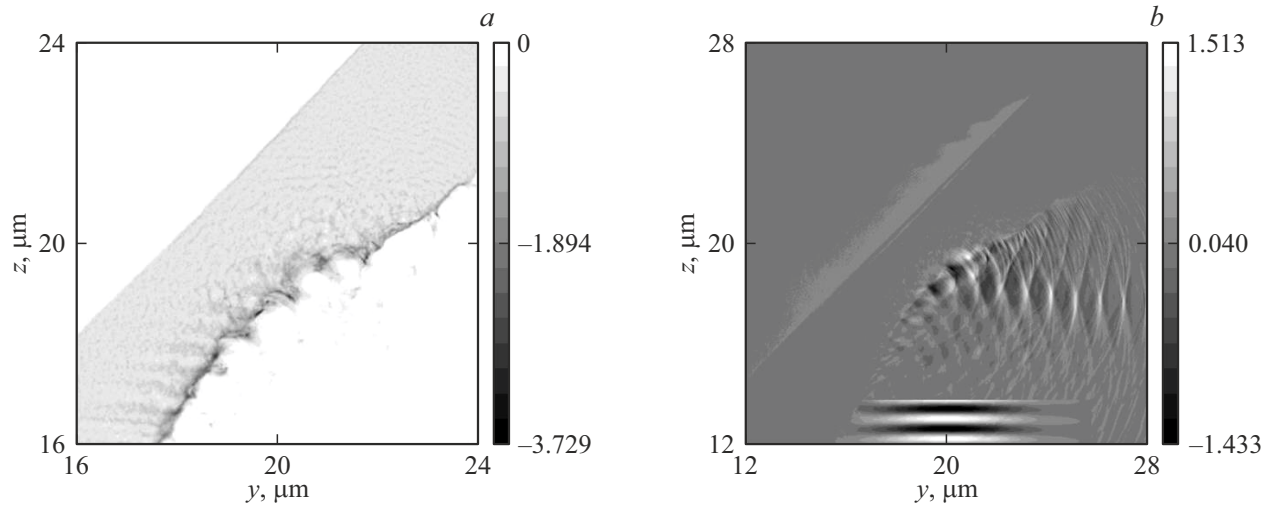

Figure 4. *a* — electron density profile, density scale in units of initial density Zn_{i0}, the negative sign corresponds to the negative charge of the electron; *b* — electric field of the incident pulse at $t = 0$ (insert below) and the reflected pulse at $t = 42$ fs for a target with a thickness of $3.5\,\mu$m and heterogeneity scale of $0.25\,\mu$m. The scale of the field strength on the right in units of the incident pulse amplitude.

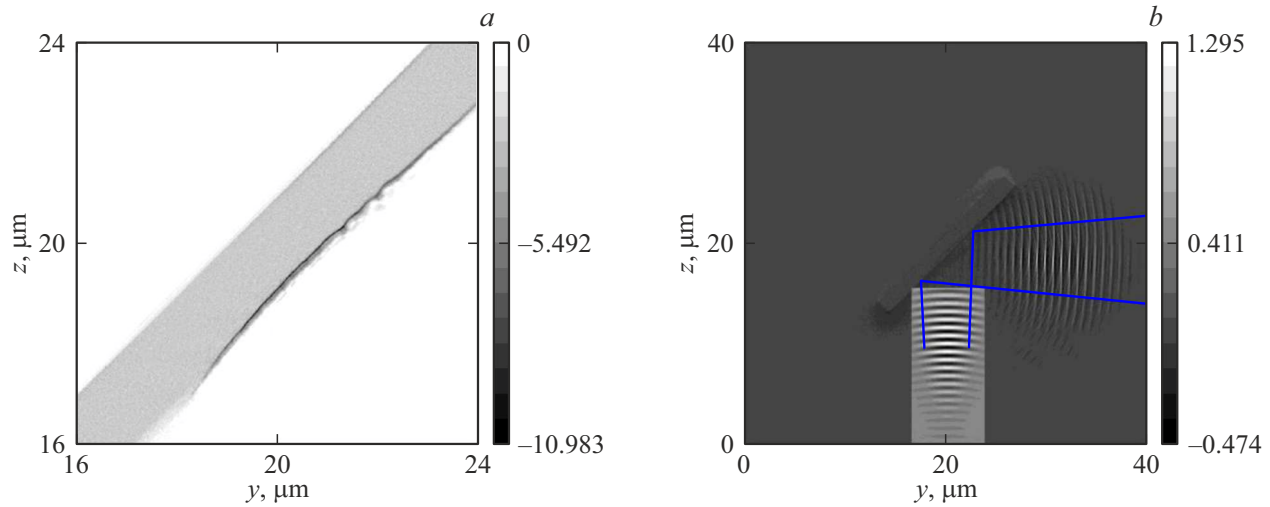

Figure 5. *a* — the electron density profile at time 90 fs (45 fs after the first laser pulse has been reflected from the target), the density scale in units of initial density Zn_{i0}, the negative sign corresponds to the negative charge of the electron, the dark line highlights the surface of critical density (reflecting surface), $I_L = 6.7 \cdot 10^{19}$ W/cm^2, $\tau_L = 33$ fs, target SiO_2, $n_{i0} = 2 \cdot 10^{22}$ cm^{-3}, Si^{+12}, O^{+8}, $L = 0.25\,\mu$m, $w_L = 1.5\,\mu$m; *b* — the electric field of the second pulse (parameters coincide with the parameters of the first one) incident on the target at time $t = 108$ fs and fully reflected at $t = 160$ fs. The scale of the field strength on the right in units of the incident pulse amplitude.

lines. By comparing Fig. 1, *a* and Fig. 5, *b* we see that the surface of local density increase for a time ~ 100 fs is featuring a smoother profile and is remained concave with a sharp boundary in Fig. 5, *a*. The electron jets shown in Fig. 1, *a* and Fig. 4, *a*, are dissipating after completion of the first pulse and the reflection surface is smoothed. Accordingly, if a second laser pulse is applied to the target again in Fig. 5, its degree of focusing can be improved. Fig. 5, *b* shows the focusing of the second pulse, which lags behind the first by 108 fs and is reflected from the density profile Fig. 5, *a*. A comparison of Fig. 4, *a* and Fig. 5, *b* demonstrates that the second pulse is broadened (compared to the first pulse) when it approaches the target because of the diffraction divergence and it also has a convex front. Focusing shown in Fig. 5, *b* causes the front of the reflected second pulse to become plane (concave). The maximum amplitude of the reflected second pulse is 1.3 in units of the amplitude of the incident second pulse. The scattered radiation of the second pulse in Fig. 6 has a strict periodic structure and does not contain the chaotic part visible in Fig. 4, *b*. To estimate the parameters of the reflecting surface profile in Fig. 5, *a*, formula (4) can be used, while in (4) the duration of the laser pulse τ_L should be replaced by the delay time $\Delta\tau = 108$ fs between

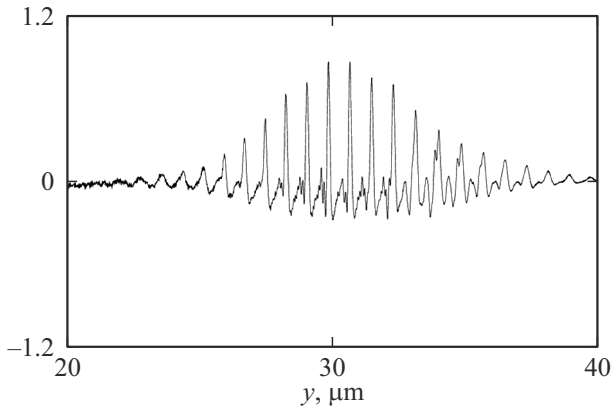

Figure 6. Electric field in the axis of the second reflected pulse ($z = 19\,\mu$m in Fig. 5, *b*). Duration of the field half-period at half maximum is 54 nm. Field strength scale in units of the incident pulse amplitude along the ordinate axis.

pulses, and the "drop" depth of the profile $z_T \approx z_i$. Here, according to formula (6), the focusing distance is estimated as $f_{pt} \approx 13\,\mu$m, which corresponds to the focusing distance $\sim 10\,\mu$m in Fig. 5, *b*. Electric field in the axis of the second reflected pulse ($z = 19\,\mu$m in Fig. 6) is shown in Fig. 6. Comparison of the atto pulses generated by the first and second laser pulses shows that the maximum amplitude of the atto pulses of the second laser pulse is higher and the duration is shorter by ~ 4 times. Thus, the profile of the focusing surface can be controlled not only by changing the scale of the density heterogeneity on the front side or by changing the laser intensity of a single pulse, but also by using a two-pulse scheme. In this scheme, the first pulse forms a curved reflection surface with high density, and the second pulse generates a set of atto pulses and becomes focused. Figure 6 illustrates that the two-pulse scheme generates atto pulses of greater amplitude and shorter duration, i.e. it is characterized by a higher quality of atto pulses.

Conclusion

The atto pulse reflected from a plasma target containing high-frequency harmonics can be focused not only using a pre-formed concave surface, but also due to self-consistency. In the latter case, the deflection of the surface occurs due to the laser radiation pressure, and the focusing parameters of the resulting concave mirror depend on the scale of laser plasma heterogeneity, the focus point of the incident pulse, and the laser intensity. The scale of plasma heterogeneity depends on the intensity and duration of the laser pre-pulse, and by selecting these parameters, it is possible to change the curvature of the reflecting surface, compensate for the diffraction divergence (curvature of the front) of the main pulse, and assign the reflected pulse focus to the given distance. Instead of changing the heterogeneity scale (changing the parameters of the pre-pulse), you can change the position of the focus point of the incident beam relative to the target surface (i.e., move the target) and also obtain the given position of the focus point of the reflected beam. By focusing, it is possible to obtain the intensity of the high-frequency harmonics of the reflected pulse at the level of the intensity of the incident laser pulse. High-frequency harmonics are featuring lower diffraction divergence, and angle selection is possible at large distances: separation of the low-frequency and high-frequency parts of the reflected pulse. The high-frequency harmonics are combined into a sequence of short intense pulses (atto pulses), so it is possible to separate the atto pulses for the purposes of X-ray methods with high time resolution. The concave reflective surface continues to form even after the first laser pulse has been reflected. The quality of such a surface is better than during the action of the pulse. The mirror formed in this way has a ready-made dense thin electronic layer, optimal for repeated generation of atto pulses. As a result, the second pulse reflected from the target is characterized by better focusing (higher amplitude and shorter duration of the atto pulses).

Funding

This study was supported by grant No.23-12-00012 from the Russian Science Foundation. Computer cluster „Polytechnic–RSK Tornado" at Peter the Great St. Pe-

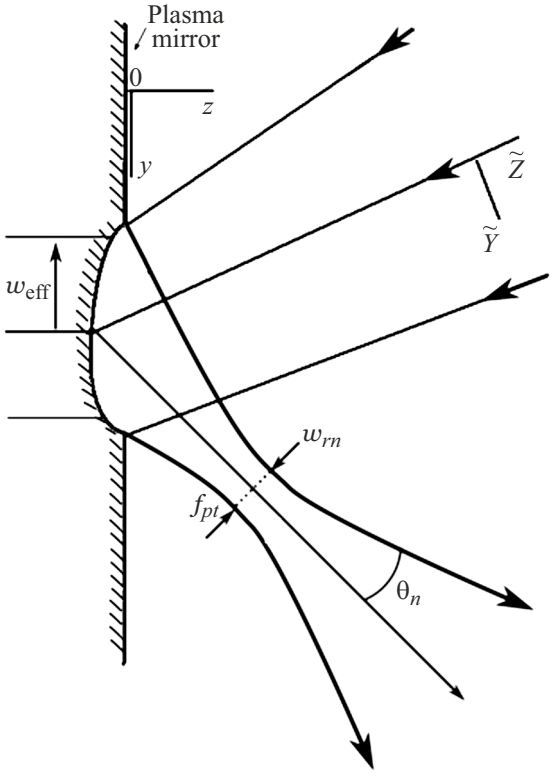

Fig. it.1. Focusing of the reflected laser pulse by a concave self-consistent plasma reflection surface.

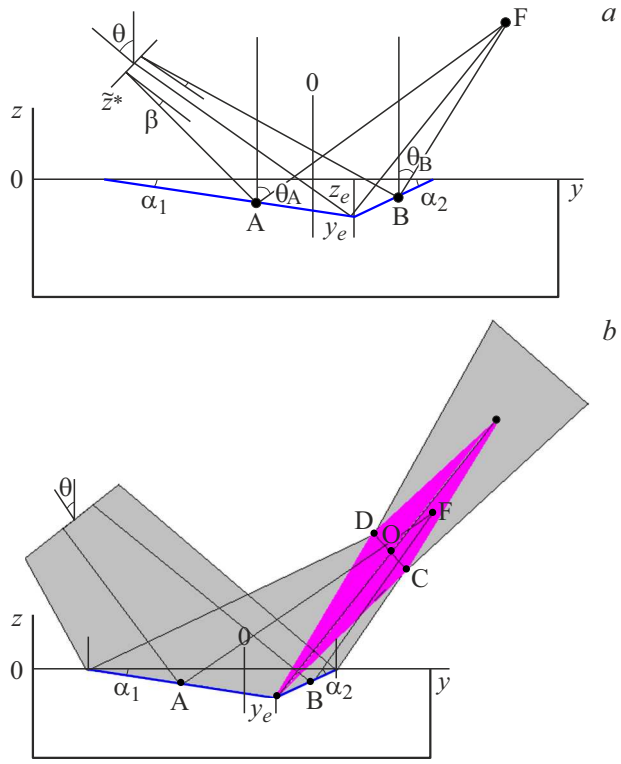

Fig. it.2. *a* — focusing in the approximation of the straightforwardly emitted rays. *b* — caustic region (lilac color) and location of the point O — focusing the reflected beam, gray color shows the incident and reflected laser field.

tersburg Polytechnic University was used for numerical computations.

Appendix 1

An obliquely incident pulse (5) with a curved front is focused by a non-ideal concave mirror with a blurred focusing distance at δf_p, as shown in Fig. p1. Let's approximate the numerically modelled reflection surface in Fig. 1, *a* with a triangular profile, as shown in Fig. p2, *a, b*. The values of the angles in Fig. p2 are determined by obvious formulas, in particular, the angles of inclination of the surface

$$\alpha_1 \approx \tan\alpha_1 = \frac{z_T}{\frac{w_L}{\cos\theta} + y_e},$$
$$\alpha_2 \approx \tan\alpha_2 = \frac{z_T}{\frac{w_L}{\cos\theta} - y_e}. \quad \text{(A1)}$$

Angle β of the laser beam divergence after the waist

$$\beta \approx \frac{z^*}{z_R \cos\theta}, \quad \text{(A2)}$$

where z^* — the height of the laser beam focusing point above the target surface. After reflection the AF and BF rays are propagating at angles $\theta_{A,B}$ to the normal line as defined from the formulae

$$\theta_A = \theta - \beta + 2\alpha_1,$$

$$\theta_B = \theta + \beta - 2\alpha_1. \quad \text{(A3)}$$

Point F of AF and BF rays intersection has the coordinates

$$z_F = \frac{w_L(\cot\theta_A \tan\alpha_2 - \cot\theta_B \tan\alpha_1)}{\cos\theta(\cot\theta_A - \cot\theta_B)}$$
$$+ \frac{y_A \cot\theta_B(\cot\theta_A - \tan\alpha_1) - y_B \cot\theta_A(\cot\theta_B + \tan\alpha_2)}{\cot\theta_A - \cot\theta_B},$$
$$y_F = \frac{w_L(\tan\alpha_2 - \tan\alpha_1)}{\cos\theta(\cot\theta_A - \cot\theta_B)}$$
$$+ \frac{y_A(\cot\theta_A - \tan\alpha_1) - y_B(\cot\theta_B + \tan\alpha_2)}{\cot\theta_A - \cot\theta_B},$$
$$y_A \in \left[-\frac{w_L}{\cos\theta}; y_e\right], \quad y_B \in \left[y_e; \frac{w_L}{\cos\theta}\right]. \quad \text{(A4)}$$

Here $y_{A,B}$ — coordinates of points A, B on the axis y. When changing the position of points A and B on the reflecting surface independently (i.e., if the coordinates $y_{A,B}$ are independently changed in the specified range (A4)), the point F will fill in the caustic region shown in Fig. p2, *b* in purple color. The reflected beam has the smallest transverse dimension at a point O with coordinates

$$z_O = \frac{w_L}{\cos\theta(\tan\theta_A - \tan\theta_B)},$$
$$y_O = \frac{w_L}{2\cos\theta} + \frac{w_L}{\cos\theta\left(\frac{\tan\theta_A}{\tan\theta_B} - 1\right)}. \quad \text{(A5)}$$

Consequently, the focusing distance of a triangular profile mirror will be

$$f_{pt} = \sqrt{z_O^2 + y_O^2} = \frac{w_L\sqrt{1 + (\tan\theta_A + \tan\theta_B)^2/4}}{\cos\theta(\tan\theta_A - \tan\theta_B)}. \quad \text{(A6)}$$

Given $\theta \gg \alpha_{1,2}, \beta$ and $\alpha_{1,2} \ll 1$, $\beta \ll 1$ the formula to find the focusing distance is simplified and Taylor expansion with respect to small $\alpha_{1,2} \ll 1, \beta \ll 1$ is written as follows

$$f_{pt} \approx \frac{w_L}{2(\alpha_1 + \alpha_2 - \beta)} = \frac{w_L}{\frac{2(z_T/(w_L/\cos\theta + y_e) +}{z_T/(w_L/\cos\theta - y_e) - z^*/z_R\cos\theta)}}. \quad \text{(A7)}$$

For X-ray methods with attosecond time resolution, the focusing distance f_{pt} should be large and reach at least hundreds of micrometers. In this case, formula (A7) allows us to determine the range of focus points of the incident beam z^*, which ensures that the set focusing distance f_{pt} of the reflected beam exceeds the set value. In the interval of the incident pulse focusing points

$$z^* \in \left[\frac{2w_L z_T z_R}{w_L^2/\cos^2\theta - y_e^2} - \frac{w_L z_R \cos\theta}{2f_{pt}}; \frac{2w_L z_T z_R}{w_L^2/\cos^2\theta - y_e^2}\right] \quad \text{(A8)}$$

the reflected laser pulse will be focused on distances higher than f_{pt}. The focus point is located on the axis of the specularly reflected pulse at a distance determined by the ratio (A7) from the target surface.

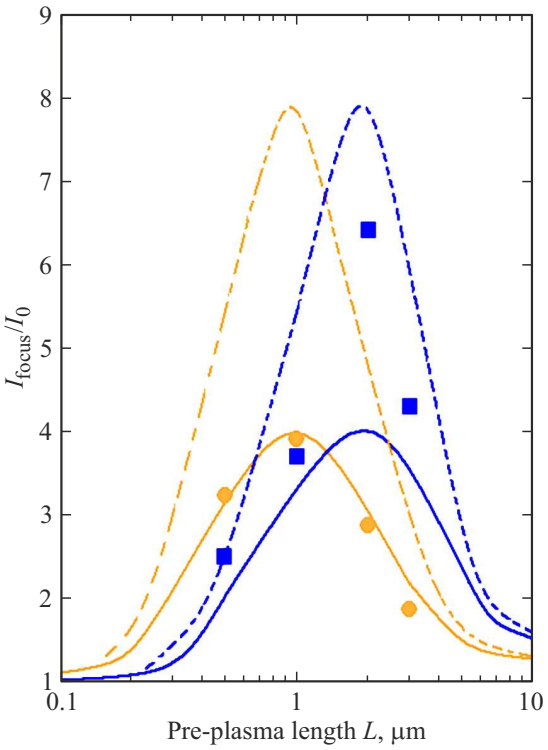

Fig. it.3. Dimensionless intensity at the point of focus f_{pt} versus plasma heterogeneity scale for the intensity of laser pulse 10^{18} W/cm^2 ($a_0 = 0.7$) — blue curve and 10^{19} W/cm^2 ($a_0 = 2.2$) — orange curve. Circles and squares — data of PIC-computation [7]. The solid curve corresponds to the triangular density profile in model (9), (10), dashed curve —corresponds to the trapezoidal profile with the same length of links. Other parameters of the target and laser pulse are shown in Fig. 2.

At $y_e = 0$ and laser pulse focusing on the surface of target ($z^* = 0$) formula (A7) leads to $f_{pt} \approx w_L^2/4z_T \cos\theta$, which corresponds to the estimates made in this paper and estimates from [1]. To estimate the intensity of the reflected focused beam let's find the size |CD| in Fig. p2, *b*. The coordinates of points C, D in Fig. p2, *b* are defined by the system (A4), where the coordinates pf point F will coincide with the coordinates of point D, if $y_A = -w_L/\cos\theta$, $y_B = y_e$. Accordingly, for the point C $y_A = y_e$, $y_B = w_L/\cos\theta$. The transverse size |CD| of the focused laser beam will be

$$|\mathrm{CD}| = 2w_{rn} = \sqrt{(z_D - z_C)^2 + (y_D - y_C)^2}$$

$$\approx w_L\left(1 + \frac{\tan(\frac{\alpha_1+\alpha_2-\beta}{2})}{\cot(\theta+\alpha_1+\alpha_2-\beta)\cos\theta}\right). \qquad \text{(A9)}$$

Appendix 2

The solid and dashed lines in Fig. p3 show the results of the model (9), (10) respectively, for the triangular profile of the reflecting surface (solid lines) and for the trapezoidal profile with the same length of all links (dashed lines). Comparison of (10) with a numerical computation [7] (circles and squares in Fig. p3) shows that for $a_0 > 1$, the triangular density profile has a better matching with the numerical computation, and for $a_0 = 0.7$, the trapezoid profile (dashed lines) gives the best consistency. Thus, the numerical modelling data shows that the shape of the surface profile depends on parameters of the problem (I_0, L). The intensity of harmonics (10) of the focused reflected pulse, in its turn, depends on the type of the surface profile.

References

[1] M.R. Edwards, J.M. Mikhailova. Sci. Rep., **10**, 5154 (2020). DOI: 10.1038/s41598-020-61255-0
[2] R. Lichters, J. Meyer-terVehn, A. Pukhov. Phys. Plasmas, **3**, 3425 (1996).
[3] P. Gibbon. *Short Pulse Laser Interactions with Matter* (Imperial College Press, 2005).
[4] H. Vincenti, S. Monchoce, S. Kahaly, G. Bonnaud, Ph. Martin, F. Quere. Nature Commun., **5**, 3403 (2014). DOI: 10.1038/ncomms4403
[5] A. Kemp, H. Ruhl. Phys. Plasmas, **12**, 033105 (2005). DOI: 10.1063/1.1856933
[6] A.A. Andreev, K.Yu. Platonov. Opt. i spektr., **114**, 859 (2013) (in Russian).
[7] H-E. Tsai, A.V. Arefiev, J.M. Shaw, D.J. Stark, X. Wang, R. Zgadzaj, M.C. Downer. Phys. Plasmas, **24**, 013106 (2017).
[8] A.A. Gonoskov, A.V. Korzhimanov, A.V. Kim, M. Marklund, A.M. Sergeev. PRE, **84**, 046403 (2011).
[9] S. Gordienko, A. Pukhov, O. Shorokhov, T. Baeva. Phys. Rev. Lett., **93**, 115002 (2004).
[10] S. Gordienko, A. Pukhov, O. Shorokhov, T. Baeva. Phys. Rev. Lett., **94**, 103903 (2005).
[11] F. Quéré, H. Vincenti. High Power Laser Science and Engineering, **9**, 13 (2021). DOI: 10.1017/hpl.2020.46
[12] H. Vincenti. Phys. Rev. Lett., **123**, 105001 (2019).

Translated by T.Zorina